Quantum interference and nonlinear optical processes in the conduction bands of infrared-coupled quantum wells

S. M. Sadeghi, S. R. Leffler, and J. Meyer
The University of British Columbia, Department of Physics and Astronomy, 6224 Agricultural Road, Vancouver, British Columbia, Canada V6T 1Z1

(Received 28 September 1998; revised manuscript received 21 January 1999)

We study quantum interference and nonlinear optical processes in the conduction band of an *n*-doped quantum well driven by one or two infrared fields. The fields couple a broad upper subband to a lower energy subband and the ground subband, forming a Λ configuration. We show, including the effect of electron-electron scattering and dynamic screening, that this configuration can lead to coherent control of the intersubband transitions, such as coherent population trapping. We also study quantum interference processes, such as laser-induced transparency and dark-line effects in the linear absorption and gain spectra of the system. The effects on these processes of differing field intensities and of electron-electron scattering are also discussed. [S0163-1829(99)04823-7]

I. INTRODUCTION

Quantum interferences in the optical interband and intersubband transitions in quantum wells (QW's) can produce exotic effects not otherwise seen in semiconductor physics, and can lead to useful applications. For example, these interferences have previously been shown to allow coherent control of electron transitions, producing photocurrents with preferred directions in bulk and QW semiconductors,[1–2] and intersubband gain via multiphoton processes.[3] They can also be used to manipulate the excitonic emission and absorption spectra of QW's.[4] In the latter study, the authors considered the interaction between an undoped QW and infrared (IR) fields polarized along its growth direction, nearly resonant with the well's conduction-subband transitions.

In this paper, we explore quantum interference effects and nonlinear optical processes in the intersubband transitions of a QW driven by two IR fields in a Λ configuration (Fig. 1). We show that in such a system a large portion of the conduction-band population can be coherently trapped in the lower two subbands. This effect, which is known in atomic physics as coherent population trapping (CPT),[5] is investigated here by studying the electron distributions in the coupled conduction subbands. This differs from the atomic case in that in QW's the electron-electron scattering processes significantly affect the intersubband transitions by making their associated dephasing rates dependent on the field intensities and frequencies.[6] This in turn alters the interaction of the fields with the QW.

This paper also includes an investigation of the effect of varying coupling field intensity on the linear absorption of a probe field that is tunable between the three transitions of the Λ system. The absorption spectra show the effects of one- and two-photon or Raman coupling in the system, and some distinctive quantum interference features such as laser-induced transparency (LIT). In the case where only the ground and third subbands are coupled, the system has an optically pumped three-level laser configuration. This differs from the configurations considered previously,[7] however, in that the lower laser level is a coupled state. This leads to a dark line or band in the gain spectrum due to quantum interference. We discuss how the latter effect and LIT are governed by electron-electron scattering in the system. The results obtained in this paper can be applied to coherent control of intersubband transitions into the continuum of a QW, efficient achievement of inversion and nonlinear gain in QW infrared and far-infrared lasers, and the development of IR detectors and other optical devices.

In Sec. II, we briefly summarize a modified version of the formalism we developed recently[3] to model strong infrared coupling of QW's. Section III contains the results for CPT in an *n*-doped QW. The linear response of this system to a weak tunable probe field is presented in Sec. IV. The dependence of this response on the relative intensities of the IR fields is discussed in Sec. V. A discussion of the system's quantum interferences and concluding remarks are presented in Secs. VI and VII, respectively.

II. REVIEW OF THEORY

We consider the conduction band of an asymmetric *n*-doped QW. As shown in Fig. 1, two laser fields with frequencies ω_1 and ω_2 couple, respectively, the first, $|1,\mathbf{k}\rangle$, and second, $|2,\mathbf{k}\rangle$, subbands of this system with the third subband, $|3,\mathbf{k}\rangle$. In the rotating wave and dipole approximations the interaction term of the Hamiltonian for this system is

$$H_\Lambda = \hbar \sum_{\mathbf{k}} \{\mu_{13} E_1(t) c^\dagger_{1,\mathbf{k}} c_{3,\mathbf{k}} + \mu_{23} E_2(t) c^\dagger_{2,\mathbf{k}} c_{3,\mathbf{k}} + \text{H.c.}\} \tag{1}$$

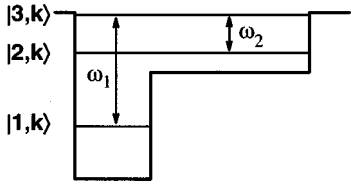

FIG. 1. Illustration of the Λ coupling configuration in an asymmetric quantum well, with infrared-field frequencies ω_1 and ω_2.

Here, the first term is the interaction term of the first field, with amplitude E_1, and the second term is that of the second field, with amplitude E_2. The μ_{ij}'s are electric dipole moments between the corresponding conduction subbands along the growth direction of the QW. These are assumed to be $\mathbf{k}$ independent. $c^{\dagger}_{i,\mathbf{k}}$ and $c_{i,\mathbf{k}}$ are creation and annihilation operators, respectively, for an electron in the ith subband with wave vector $\mathbf{k}$.

The equation of motion for the density matrix $\rho^{\mathbf{k}}$ is

$$\frac{\partial \rho^{\mathbf{k}}}{\partial t} = -\frac{i}{\hbar}[H_0 + H_\Lambda, \rho^{\mathbf{k}}] + \left.\frac{\partial \rho^{\mathbf{k}}}{\partial t}\right|^{\text{incoh}}_{e-e} + \left.\frac{\partial \rho^{\mathbf{k}}}{\partial t}\right|^{\text{incoh}}_{e-p}. \quad (2)$$

Here, H_0 is the Hamiltonian of the QW in the absence of any IR fields. The second and third terms are the incoherent contributions of the electron-electron and electron-phonon scattering processes to the system's dynamics. These terms are responsible for damping of the system. The electron density is assumed to be high here, therefore, the dynamic screening will be strong. As a result, we only consider the dephasing terms caused by these processes, which are diagonal in k space.[8] We have also ignored electron-electron scattering between electrons in different conduction subbands, because the energy spacings between the subbands are considered to be large.[9] Also the damping rates caused by the electron-electron scattering processes in the upper subbands are ignored, because (i) the upper subbands are separated from each other and the ground subband by energies greater than that of LO phonons and therefore excited electrons are affected by the very fast electron LO-phonon scattering process, and (ii) the electron envelope functions in the upper subbands are asymmetric and very much less localized in the well than those in the ground subband.

Since in this paper we consider a heavily doped asymmetric quantum well structure, the Hartree contribution dominates over the exchange-correlation term.[10] (See also Ref. 11.) The transition linewidths considered here are relatively large and become larger as the field intensities increase, however. Because of this and the fact that we consider resonant coupling, the Hartree potential does not have a significant effect. Depolarization can also renormalize the transition energies. This depends primarily on the electron density, however. Since this remains nearly constant through the coupling processes,[12] one can account for depolarization by introducing a phenomenological shift in the transition energies.

As shown in Ref. 6, in the high-excitation regime the electron-electron scattering processes in the ground conduction subband alter the intersubband transition rates. The incoherent contribution of the electron-electron scattering in this subband should therefore be treated using the Boltzmann equation

$$\left.\frac{d\rho^{\mathbf{k}}_{11}}{dt}\right|^{\text{incoh}}_{e-e} = \Gamma^{\text{in}}_1(\mathbf{k},\rho^{\mathbf{k}}_{11})(1-\rho^{\mathbf{k}}_{11}) - \Gamma^{\text{out}}_1(\mathbf{k},\rho^{\mathbf{k}}_{11})\rho^{\mathbf{k}}_{11}. \quad (3)$$

Here, $\Gamma^{\text{in}}_1(\mathbf{k},\rho^{\mathbf{k}}_{11})$ and $\Gamma^{\text{out}}_1(\mathbf{k},\rho^{\mathbf{k}}_{11})$ are the scattering in and out rates at $|1,\mathbf{k}\rangle$ due to the electron-electron scattering process. They are given by

$$\Gamma^{\text{in}}_1(\mathbf{k},\rho_{11}) = \frac{4\pi}{\hbar}\sum_{\mathbf{p},\mathbf{q}} \rho^{\mathbf{p}}_{11}\rho^{\mathbf{k}-\mathbf{q}}_{11}(1-\rho^{\mathbf{p}-\mathbf{q}}_{11})|V(q,\hbar\omega')|^2 \times \delta[E^c(1,\mathbf{k}) + E^c(1,\mathbf{p}-\mathbf{q}) - E^c(1,\mathbf{k}-\mathbf{q}) - E^c(1,\mathbf{p})], \quad (4)$$

and

$$\Gamma^{\text{out}}_1(\mathbf{k},\rho_{11}) = \frac{4\pi}{\hbar}\sum_{\mathbf{p},\mathbf{q}} (1-\rho^{\mathbf{p}}_{11})\rho^{\mathbf{p}-\mathbf{q}}_{11}(1-\rho^{\mathbf{k}-\mathbf{q}}_{11})|V(q,\hbar\omega')|^2 \times \delta[E^c(1,\mathbf{k}) + E^c(1,\mathbf{p}-\mathbf{q}) - E^c(1,\mathbf{k}-\mathbf{q}) - E^c(1,\mathbf{p})]. \quad (5)$$

Here, $E^c(1,\mathbf{k})$ is the energy of an electron in the ground subband with wave vector $\mathbf{k}$ and $V(q,\hbar\omega')$ is the screened electron-electron interaction given by

$$V(q,\hbar\omega') = \frac{v_q F(q)}{\epsilon(q,\hbar\omega')}. \quad (6)$$

Here, $v_q = 2\pi e^2/(Sq\epsilon_b)$, e is the electronic charge, S the area of the quantum well, and ϵ_b is the bulk dielectric constant, which is assumed to be the same in the quantum well and in the barrier. Also $\hbar\omega' = E^c(1,\mathbf{k}-\mathbf{q}) - E^c(1,\mathbf{k})$, $F(q)$ is the form factor, and $\epsilon(q,\hbar\omega')$ is the dynamic dielectric function due to the quasi-two-dimensional electron gas.[6]

The polarization dephasing rates associated with the ground to upper subband transitions are strongly affected by electron-electron scattering and by the field frequencies and intensities. These rates are given by

$$\gamma^{e-e}_{12}(k) = \gamma^{e-e}_{13}(k) = \tfrac{1}{2}[\Gamma^{\text{in}}_1(k) + \Gamma^{\text{out}}_1(k)]. \quad (7)$$

Adding the contribution of the electron-phonon scattering processes (γ^p_{1j}) to these rates gives the total dephasing rates associated with the transitions between the ground and the upper subbands.

To make the system dynamics tractable and to emphasize the effects of electron-electron scattering, we consider QW structures where the energies corresponding to the 1-3 and 2-3 transitions (E_{13} and E_{23}) are integer multiples of the LO-phonon energy. This means that after an electron decays by intersubband electron LO-phonon scattering, it will undergo intrasubband scattering with LO phonons until it ends up in a state with the same wave vector as the initial state. Since these intrasubband interactions are very fast we may impose the condition $\Sigma_i \rho^{\mathbf{k}}_{ii} \simeq \rho^{0\mathbf{k}}_{11}$, where $\rho^{0\mathbf{k}}_{11}$ is the Fermi distribution. The equations of motion of the system [Eq. (2)] then become linear, and have a steady-state solution of the form

$$\rho^{\mathbf{k}}_{ij} = -\sum_{lm} (\mathbf{M}^{\mathbf{k}})^{-1}_{ij,lm}\mathbf{N}^{\mathbf{k}}_{lm}, \quad (8)$$

where $\mathbf{M}^{\mathbf{k}}$ and $\mathbf{N}^{\mathbf{k}}$ are tensors containing the coefficients of the equations of motion and i, j, l, and m run over all subband indices.[3] This allows the steady-state electron distributions and electron-electron scattering rates to be calculated iteratively.

To obtain the linear response of the system to a weak probe field, we apply the quantum regression theorem. The

contributions to the linear absorption spectrum of the system due to the 1–2, 2–3, and 1–3 transitions are given by

$$A_{12}^{\Lambda}(\omega_p)=\mu_{12}^2\,\mathrm{Re}\sum_{\mathbf{k}}\rho_{11}^{\mathbf{k}}\{[R_{13,33}^{\mathbf{k}}(z)-R_{13,11}^{\mathbf{k}}(z)-R_{13,12}^{\mathbf{k}}(z)]\rho_{31}^{\mathbf{k}}+R_{13,23}^{\mathbf{k}}(z)\rho_{21}^{\mathbf{k}}+R_{13,13}^{\mathbf{k}}(z)[\rho_{11}^{\mathbf{k}}-\rho_{33}^{\mathbf{k}}]\},\tag{9}$$

$$A_{23}^{\Lambda}(\omega_p)=\mu_{23}^2\,\mathrm{Re}\sum_{\mathbf{k}}\rho_{22}^{\mathbf{k}}\{[R_{32,22}^{\mathbf{k}}(z')-R_{32,33}^{\mathbf{k}}(z')]\rho_{23}^{\mathbf{k}}+R_{32,32}^{\mathbf{k}}(z')\rho_{33}^{\mathbf{k}}+R_{32,12}^{\mathbf{k}}(z')\rho_{13}^{\mathbf{k}}-R_{32,32}^{\mathbf{k}}(z')\rho_{22}^{\mathbf{k}}-R_{32,31}^{\mathbf{k}}(z')\rho_{21}^{\mathbf{k}}\},\tag{10}$$

and

$$A_{13}^{\Lambda}(\omega_p)=\mu_{13}^2\,\mathrm{Re}\sum_{\mathbf{k}}\rho_{11}^{\mathbf{k}}\{[R_{12,22}^{\mathbf{k}}(z'')-R_{12,11}^{\mathbf{k}}(z'')]\rho_{21}^{\mathbf{k}}+[\rho_{11}^{\mathbf{k}}-\rho_{22}^{\mathbf{k}}]R_{12,12}^{\mathbf{k}}(z'')+R_{12,32}^{\mathbf{k}}(z'')\rho_{31}^{\mathbf{k}}-R_{12,13}^{\mathbf{k}}(z'')\rho_{23}^{\mathbf{k}}\}.\tag{11}$$

Here, $z=i(\omega_p-\omega_1+\omega_2)$, $z'=i(\omega_p-\omega_2)$, and $z''=i(\omega_p-\omega_1)$. Also,

$$R_{ij,lm}^{\mathbf{k}}(z)=(z\mathbf{I}-\mathbf{M}^{\mathbf{k}})_{ij,lm}^{-1},\tag{12}$$

where $\mathbf{I}$ is the identity tensor with the same dimensions as $\mathbf{M}^{\mathbf{k}}$.

In practice, observation of the phenomena predicted in this paper would require the use of pulsed rather than continuous-wave infrared lasers for the coupling fields. The steady-state model used here is valid as long as the infrared pulses are much longer than the largest damping time of the system, i.e., $\tau_p \gg 1/\gamma_{12}$. Since $5 \leqslant \gamma_{12} \leqslant 15\ \mathrm{ps}^{-1}$ for the whole range of field intensities considered, subnanosecond pulses can be used without invalidating the model.

III. COHERENT POPULATION TRAPPING IN QW's

To study CPT in QW's, we consider a structure that contains a 3.8-nm GaAs layer followed by 8-nm $Al_{0.25}Ga_{0.75}As$, confined by $Al_{0.39}Ga_{0.61}As$ barriers. In this structure, $E_{13}=214$ and $E_{23}=73$ meV, both of which are nearly integer multiples of the LO-phonon energy. We assume that this structure is *n*-doped to give an electron density of $7.3\times10^{11}\ \mathrm{cm}^{-2}$, and consider $\mu_{12}=e\times1.02$, $\mu_{13}=e\times0.92$, and $\mu_{23}=e\times2.55$ nm. The damping rates of $|2,\mathbf{k}\rangle$ and $|3,\mathbf{k}\rangle$ are considered to be $\Gamma_2^p=5$ and $\Gamma_3^p=30\ \mathrm{ps}^{-1}$, respectively. The effective mass for each layer is obtained from $m^*=[0.067(1-x)+0.15x]m_e$, where x is the fraction of Al present and m_e is the free-electron mass.[13] The temperature of the QW is considered to be 4 K.

Figure 2(a) shows the evolution of ρ_{ii}^k ($i=1$, 2, and 3) at $k=k_f$ for $\Omega_{13}=\Omega_{23}=20\ \mathrm{ps}^{-1}$ (corresponding to IR intensities of 113 and 14.9 MW/cm^2, respectively), $\Delta_2=0$, and various Δ_1. Here, $\Omega_{j3}\equiv-\mu_{j3}E_j/\hbar$. is the Rabi frequency and Δ_j is the detuning of the coupling field with frequency ω_j. For $|\Delta_1|\gg0$, the system dynamics are dominated by one-photon transitions of electrons into the second and third subbands and energy relaxation of electrons from the latter to the former. As a result, the electron populations reflect the subbands' widths and energies. As $|\Delta_1|$ decreases, however, the population in the third subband becomes depleted despite the enhancement of the 1–3 coupling strength (dotted line). The ground subband population (solid line) increases, and when $\Delta_1=0$ most of the electron population is divided between the ground and second subbands.

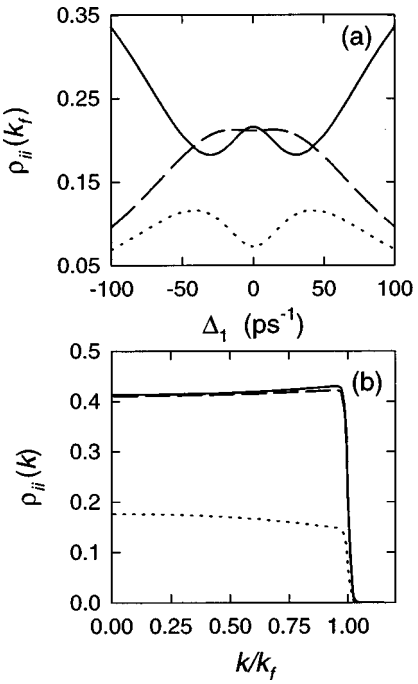

FIG. 2. Electron distributions in a Λ system with $\Omega_{13}=\Omega_{23}=20\ \mathrm{ps}^{-1}$. (113 MW/cm^2 at frequency ω_1 and 14.9 MW/cm^2 at ω_2). The solid, dashed, and dotted lines represent the populations in the first, second, and third subbands, respectively. (a) The effect of detuning one of the coupling fields on the Fermi-level populations ($k=k_f$). (b) The complete electron distributions in the resonant coupling case.

To understand these results, note that the coupling mechanisms of a Λ system are in general one-photon coupling of all three subbands and two-photon or Raman coupling of $|1,\mathbf{k}\rangle$ and $|2,\mathbf{k}\rangle$ through $|3,\mathbf{k}\rangle$.[14] In a dressed state picture when the fields are resonant with their corresponding transitions, the states associated with these mechanisms at $|1,\mathbf{k}\rangle$ are the one-photon states,[15]

$$|1,t\rangle_{\mathbf{k}}=\frac{1}{\sqrt{2}}[\cos\beta|1,n\omega_1,n'\omega_2\rangle_{\mathbf{k}}-|2,(n-1)\omega_1,(n'+1)\omega_2\rangle_{\mathbf{k}}+\sin\beta|3,(n-1)\omega_1,n'\omega_2\rangle_{\mathbf{k}}],\tag{13}$$

$$|1,s\rangle_{\mathbf{k}}=\frac{1}{\sqrt{2}}[\cos\beta|1,n\omega_1,n'\omega_2\rangle_{\mathbf{k}}+|2,(n-1)\omega_1,(n'+1)\omega_2\rangle_{\mathbf{k}}+\sin\beta|3,(n-1)\omega_1,n'\omega_2\rangle_{\mathbf{k}}],\tag{14}$$

and the two-photon state

$$|1,r\rangle_{\mathbf{k}}=[-\sin\beta|1,n\omega_1,n'\omega_2\rangle_{\mathbf{k}} + \cos\beta|2,(n-1)\omega_1,(n'+1)\omega_2\rangle_{\mathbf{k}}]. \quad (15)$$

Here,

$$\tan\beta=\frac{\Omega_{23}}{\Omega_{13}}, \quad (16)$$

and n and n' are the photon numbers at frequencies ω_1 and ω_2, respectively.

Similarly, the dressed states associated with $|2,\mathbf{k}\rangle$ are

$$|2,t\rangle_{\mathbf{k}}=\frac{1}{\sqrt{2}}[\cos\beta|1,(n+1)\omega_1,(n'-1)\omega_2\rangle_{\mathbf{k}} - |2,n\omega_1,n'\omega_2\rangle_{\mathbf{k}}+\sin\beta|3,n\omega_1,(n'-1)\omega_2\rangle_{\mathbf{k}}], \quad (17)$$

$$|2,s\rangle_{\mathbf{k}}=\frac{1}{\sqrt{2}}[\cos\beta|1,(n+1)\omega_1,(n'-1)\omega_2\rangle_{\mathbf{k}} + |2,n\omega_1,n'\omega_2\rangle_{\mathbf{k}}+\sin\beta|3,n\omega_1,(n'-1)\omega_2\rangle_{\mathbf{k}}], \quad (18)$$

and

$$|2,r\rangle_{\mathbf{k}}=[-\sin\beta|1,(n+1)\omega_1,(n'-1)\omega_2\rangle_{\mathbf{k}} + \cos\beta|2,n\omega_1,n'\omega_2\rangle_{\mathbf{k}}], \quad (19)$$

and for $|3,\mathbf{k}\rangle$

$$|3,t\rangle_{\mathbf{k}}=\frac{1}{\sqrt{2}}[\cos\beta|1,(n+1)\omega_1,n'\omega_2\rangle_{\mathbf{k}} - |2,n\omega_1,(n'+1)\omega_2\rangle_{\mathbf{k}}+\sin\beta|3,n\omega_1,n'\omega_2\rangle_{\mathbf{k}}], \quad (20)$$

$$|3,s\rangle_{\mathbf{k}}=\frac{1}{\sqrt{2}}[\cos\beta|1,(n+1)\omega_1,n'\omega_2\rangle_{\mathbf{k}} + |2,n\omega_1,(n'+1)\omega_2\rangle_{\mathbf{k}}+\sin\beta|3,n\omega_1,n'\omega_2\rangle_{\mathbf{k}}], \quad (21)$$

and

$$|3,r\rangle_{\mathbf{k}}=[-\sin\beta|1,(n+1)\omega_1,n'\omega_2\rangle_{\mathbf{k}} + \cos\beta|2,n\omega_1,(n'+1)\omega_2\rangle_{\mathbf{k}}]. \quad (22)$$

Since for the system of Fig. 2(a) the intermediate state $|3,\mathbf{k}\rangle$ is relatively broad, when $|\Delta_1|\gg 0$ both forms of coupling are suppressed, and transitions between pairs of states are dominant. When Δ_1 becomes close to zero, however, two-photon coupling becomes more significant and the population is transferred into $|1,r\rangle_{\mathbf{k}}$ and $|2,r\rangle_{\mathbf{k}}$, i.e., CPT occurs. The breadth of the intermediate state has a strong effect on the efficiency of CPT, since it causes suppression of one-photon coupling compared to two-photon coupling.

Figure 2(b) shows the complete electron distributions in the three coupled conduction subbands for $\Delta_1=\Delta_2=0$ and $\Omega_{13}=\Omega_{23}=20\,\mathrm{ps}^{-1}$. Under these conditions the populations in the first and second subbands are virtually equal, each being over 40% of the total. The slight nonflatness in the distributions is caused by the k-dependent effect of electron-electron scattering on the intersubband dephasing rates (see Fig. 4). The scattering is enhanced here since the ground subband distribution is significantly different from the Fermi distribution.[6]

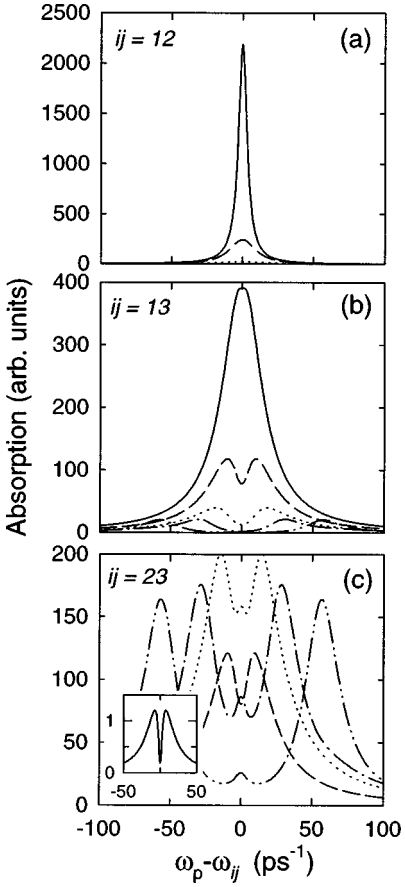

FIG. 3. Linear absorption of a weak probe field in a resonantly coupled Λ system. Parts (a), (b), and (c) show, respectively, the contributions due to the 1-2, 1-3, and 2-3 transitions. The Rabi frequencies corresponding to each line are solid: $\Omega=1$ ps^{-1}; dashed: $\Omega=5$ ps^{-1}; dotted: $\Omega=10$ ps^{-1}; dash-dotted: $\Omega=20$ ps^{-1}; dash-dot-dotted: $\Omega=40$ ps^{-1}.

IV. LINEAR ABSORPTION SPECTRA OF A QUANTUM WELL Λ SYSTEM

In the preceding section we studied the electron distributions of an IR-coupled QW system with a Λ configuration. In this section, we investigate the linear absorption spectra [Eqs. (9)–(11)] of this system when $\Omega_{13}=\Omega_{23}\equiv\Omega$. The structure considered is the same as in the preceding section.

As Fig. 3(a) shows, when Ω increases from 1 to 5 ps^{-1} the absorption due to the 1-2 transition is strongly suppressed. For $\Omega=20$ ps^{-1} [the condition of Fig. 2(a)] and higher the absorption virtually vanishes. This strong suppression occurs because most of the electron population is equally distributed between the first and second subbands due to CPT [Fig. 2(b)].

The effects of CPT are seen in other parts of the absorp-

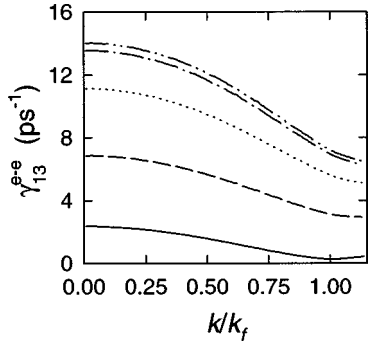

FIG. 4. Electron-electron scattering contribution to the polarization dephasing rate of the 1-3 transition. The curves are for the same conditions as those in Fig. 3.

tion spectrum as well. At $\Omega=5\ \mathrm{ps}^{-1}$, the contribution due to the 1-3 transition becomes doubled, as Fig. 3(b) shows. For higher field intensities the two peaks become smaller and move away from the central frequency. These changes occur because when CPT happens, the ground population decreases from a Fermi distribution to a non-Fermi one with approximately 40% of the total population [Fig. 2(b)]. This tends to suppress the 1-3 absorption, but since the third subband is simultaneously losing its population to the other subbands, the absorption due to this transition remains noticeable. The doubling seen here is the result of transitions between the two-photon state in the ground subband ($|1,r\rangle_{\mathbf{k}}$) and the two one-photon states in the third subband ($|3,s\rangle_{\mathbf{k}}$ and $|3,t\rangle_{\mathbf{k}}$). Under resonant coupling, $|1,r\rangle_{\mathbf{k}}$ has the same energy as the uncoupled ground subband, and $|3,s\rangle_{\mathbf{k}}$ and $|3,t\rangle_{\mathbf{k}}$ have energies $\hbar\sqrt{\Omega_{13}^2+\Omega_{23}^2}$ above and below that of the uncoupled third subband, respectively.[3] The one-photon states have less population than the two-photon state due to the dominance of two-photon coupling.

The 2-3 transition's contribution [Fig. 3(c)] shows features that reflect the evolution of the 1-3 transition's dephasing rate [$\gamma_{13}^{e-e}(k)$] with varying field intensity. For $\Omega=1\ \mathrm{ps}^{-1}$ (inset), the spectrum shows a well-resolved LIT effect. As the field intensities increase the transparency hole diminishes and then is replaced by another hole with a small peak at its center. To explain these phenomena we show in Fig. 4 the evolution of $\gamma_{13}^{e-e}(k)$ for various field intensities. For $\Omega=1\ \mathrm{ps}^{-1}$, γ_{13}^{e-e} is small, especially for states with k close to k_f. The coupling between the first and third subbands is therefore much stronger than that between the third and second. As a result, when one probes the 2-3 transition one sees a LIT effect similar to those studied in atomic or QW systems.[16–17] In such systems a narrow or metastable state is coupled into the upper level of a transition. When this transition is detected by a probe field, a transparency hole is generated in its absorption spectrum. We discuss this effect in terms of quantum interferences in Sec. VI.

Figure 4 shows that when Ω increases γ_{13}^{e-e} becomes larger, and therefore, the ground subband is no longer narrow. The fields then tend to couple the first and second subbands to the third one with comparable strengths. This establishes the two-photon coupling and CPT. Near $\Omega=5\ \mathrm{ps}^{-1}$ the mechanism of doublet generation in the 2-3 transition spectrum [Fig. 3(c)] changes from weak detection of a strongly driven two-subband system, as discussed above, to

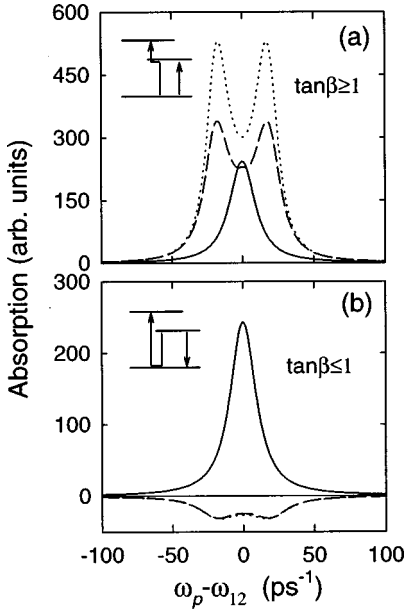

FIG. 5. The contribution of the 1-2 transition to the linear absorption of a weak probe field. In both parts, the solid line corresponds to $\Omega_{13}=\Omega_{23}=5\ \mathrm{ps}^{-1}$. In (a) the dashed line is for $\Omega_{13}=5$ and $\Omega_{23}=20\ \mathrm{ps}^{-1}$, and the dotted line is for $\Omega_{13}=0$ and $\Omega_{23}=20\ \mathrm{ps}^{-1}$. In (b) the dashed line is for $\Omega_{13}=20$ and $\Omega_{23}=5\ \mathrm{ps}^{-1}$, and the dotted line is for $\Omega_{13}=20\ \mathrm{ps}^{-1}$ and $\Omega_{23}=0$. The insets show the interfering paths that lead to LIT or dark-line generation.

transitions between multiphoton dressed states. As in Fig. 3(b), the doublet here is the result of weak detection of the two one-photon states from the two-photon state in the second subband ($|2,r\rangle_{\mathbf{k}}$). The small central peak in the latter case might be the result of electron distribution evolution and vanishes in the high-field limit.

V. FIELD-INTENSITY EFFECTS ON THE COHERENT PROCESSES

The effects studied in the previous sections were associated with equal Rabi frequencies. One feature of the Λ system, however, is that one can vary the frequencies and intensities of the fields without violating the assumptions of the theory. This allows one to explore the rich variety of nonlinear effects caused by quantum interference. In this section, we study the case where $\Omega_{13}\neq\Omega_{23}$ but the fields remain resonant with the corresponding transitions. One significant effect of this is field-coherence destruction. As Eqs. (13)–(22) indicate, large or small values of Ω_{23}/Ω_{13} cause one state to be decoupled from the rest of the system. The stronger field thus destroys the coherences generated by the weaker field, regardless of the absolute values of the field intensities.

The impact of field-coherence destruction on the 1-2 transition of the Λ system is shown in Fig. 5. The solid line in Fig. 5(a) shows the linear response due to the 1-2 transition when $\Omega_{13}=\Omega_{23}=5\ \mathrm{ps}^{-1}$ ($\tan\beta=1$). When Ω_{23} is increased by four times ($\tan\beta=4$), the spectrum becomes a doublet (dashed line). Comparing this spectrum with that for $\Omega_{23}=20\ \mathrm{ps}^{-1}$ and $\Omega_{13}=0$ (dotted line) illustrates that increasing Ω_{23} decreases the effect of the weaker field resonant with the 1-3 transition. This reduces the excitation of electrons out of

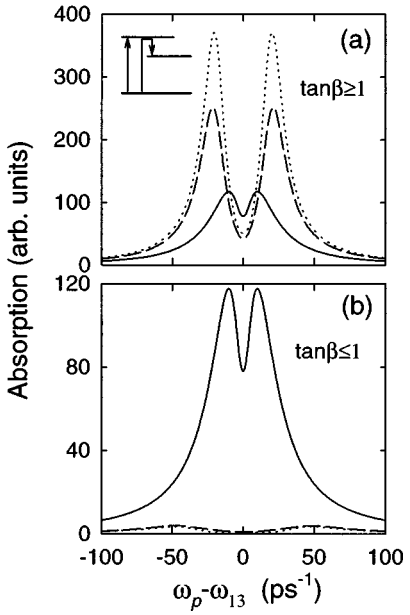

FIG. 6. The contribution of the 1-3 transition to the linear absorption of a weak probe field. The curves represent the same conditions as those in Fig. 5. The inset in (a) shows the interfering paths which lead to LIT in the spectrum shown.

the ground subband, increasing the absorption amplitude associated with the 1-2 transition. The doubling of the peak seen in Fig. 5(a) indicates the start of LIT, as will be discussed in Sec. VI, below.

Figure 5(b) shows the inverse case for the same transition, i.e., $\Omega_{13} \geqslant \Omega_{23}$. Here again the solid line corresponds to $\Omega_{13}=\Omega_{23}=5\ \mathrm{ps}^{-1}$. When Ω_{13} increases to 20 ps^{-1} ($\tan\beta = 1/4$), the spectrum changes drastically, showing extensive gain with a dip at the line center. This spectrum is almost indistinguishable from that for the case where $\Omega_{13} = 20\,\mathrm{ps}^{-1}$ and $\Omega_{23}=0$ (dotted line). In both cases, the gain is due to optical pumping of the third subband by the field with frequency ω_1, and the subsequent fast decay of the photoexcited electrons into the second subband through LO-phonon emission. Since Ω_{13} is comparable to the widths of the first and third subbands here, the stimulated emission transition is from the bare second subband into a dressed subband, which produces the hole in the gain spectrum. This will be discussed further in the following section.

Now consider the evolution of the 1-3 transition's spectrum under the same conditions as Fig. 5. As shown in Fig. 6(a) [and Fig. 3(b)], in this case when $\Omega_{23}=\Omega_{13}=5\ \mathrm{ps}^{-1}$ the 1-3 transition spectrum exhibits a transparency hole. When Ω_{23} is increased, the absorption amplitude increases and the hole becomes deeper. As was the case in Fig. 5(a), this is caused by quantum interferences that occur when the coherences involving the ground subband are destroyed. Figures 5(a) and 6(a) thus provide complementary information about the evolution of LIT in the two driven subbands of a single system. The LIT effect is weaker in the absorption associated with transitions to the narrower subband [Fig. 5(a)], because differences in the damping rates of the coupled subbands suppress (enhance) the quantum interferences that cause LIT when the narrower (broader) subband is probed. The interference processes are discussed further in the following section.

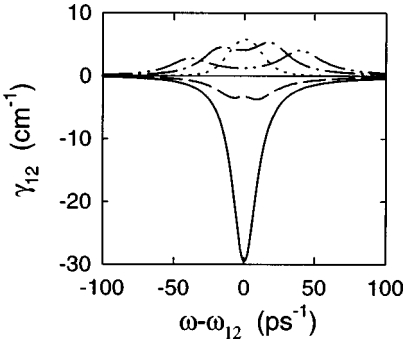

FIG. 7. The contribution of the 2-1 transition to the optical gain when only the first and third subbands are coupled. The Rabi frequencies corresponding to each line are solid: $\Omega_{13}=5\ \mathrm{ps}^{-1}$; dashed: $\Omega_{13}=7\ \mathrm{ps}^{-1}$; dotted: $\Omega_{13}=10\ \mathrm{ps}^{-1}$; dash-dotted: $\Omega_{13}=20\ \mathrm{ps}^{-1}$; dash-dot-dotted: $\Omega_{13}=40\,\mathrm{ps}^{-1}$.

Figure 6(b) shows the evolution of the absorption due to the 1-3 transition, under the same conditions as Fig. 5(b). While the latter shows a large amount of gain, here we only see a doublet, which is suppressed with increasing field strength. This suppression is caused by deposition of most of the electrons in the second subband. The system consisting of the two driven subbands here is similar to that discussed in detail in Ref. 6.

VI. QUANTUM INTERFERENCES IN A Λ SYSTEM

Quantum interferences in the intersubband transitions are primarily determined by the coupling mechanisms and configuration of the system.[18] The relative strengths of the coupling mechanisms depend on the coupled subband widths and the field frequencies and intensities. We showed in the previous section that when one field was either weaker than the other or was absent altogether, quantum interferences could lead to LIT and dark-line effects. In this section we discuss these effects in more detail.

The quantum interferences in Figs. 5 and 6 are mainly determined by one-photon coupling of two conduction subbands, and the probe transitions. There are two types of interfering paths: direct ones created by the probe field, and indirect ones generated by both the probe and coupling fields. In the case of Fig. 5(a) the direct path is the 1-2 transition, and the indirect one is the 1-3 transition through 2 [see Fig. 5(a) inset]. The interference paths for the inverse case [Fig. 5(b)] are similar in origin, but the intermediate state of the indirect path is the ground subband (see inset). These interferences generate fixed-frequency LIT or dark-line effects, depending on the population of the driven subbands.

The dynamics of the gain in Fig. 5(b) are made clearer by considering various values of Ω_{13} with $\Omega_{23}=0$. To allow easier comparison with other systems,[7,19] Fig. 7 shows the contribution of the 1-2 transition to the optical gain of a single quantum well,

$$\gamma_{12}(\omega) = -\omega\sqrt{\frac{\mu_0}{\epsilon_0}}\frac{1}{\pi\epsilon_b^{3/2}L_{\mathrm{eff}}}\,\mathrm{Im}\int_0^{k_{\max}} k\,dk \times \frac{|\mu_{12}|^2(\rho_{11}^k-\rho_{22}^k)}{\hbar\{\Delta_1 - i[\gamma_{12}^{e-e}(k)+\gamma_{12}^{p}]\}}. \tag{23}$$

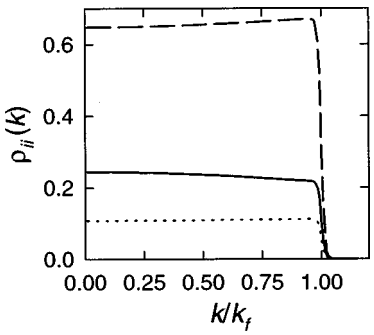

FIG. 8. Electron distributions for the system of Fig. 7, with $\Omega_{13}=20$ ps^{-1} ($I=113$ MW/cm^2). The solid, dashed, and dotted lines represent the populations in the first, second, and third subbands, respectively.

Here, μ_0 and ϵ_0 are the permeability and permittivity of free space, respectively, and L_{eff} is the effective length over which the interaction occurs, taken to be the width of the QW. Electron-electron scattering affects the gain through the dependence of γ_{12} on ρ_{ii}^k and $\gamma_{12}^{e-e}(k)$.

For small values of Ω_{13}, there is a large absorption peak corresponding to the 1-2 transition (Fig. 7). As Ω_{13} increases, the peak is suppressed and eventually develops a transparency hole. Further increase in Ω_{13} produces a single gain peak, which develops a dark line. This illustrates the fact that quantum interferences can cause both LIT and dark-line effects in the same system, depending on the populations of the upper subbands and on the field intensities. The frequencies of the gain maxima can be tuned by changing the intensity of the field associated with Ω_{13}. For the present structure the gain mostly falls in the midinfrared. The peak gain shown in Fig. 7 is larger than the maximum achievable gain for the four-level laser system of Ref. 19, with one quantum well.

Figure 8 shows the electron distributions in the three subbands for the case where $\Omega_{13}=20\,\text{ps}^{-1}$. The second subband (dashed line) contains a large fraction of the total population—more than twice that in the ground subband (solid line).

The interferences affecting the spectra in Fig. 6(a) are between the direct 1-3 and indirect 1-3-2 paths, as shown in the inset. In the case of Fig. 6(b), however, increasing Ω_{13} suppresses the indirect path. Therefore, the system becomes similar to a driven two-subband system as discussed in Ref. 6. Here, various gain and absorption transitions give rise to spectra similar to those discussed by Mollow for atomic systems.[20]

The formalism used in this paper remains valid if $|3,\mathbf{k}\rangle$ is taken to be a quasibound subband or even unstructured conduction-band continuum, allowing coherent control of the energy spectrum of photoexcited electrons in the continuum. This is similar to the saturated laser-induced continuum structure process, which has been studied in atomic systems.[21]

VII. CONCLUSION

In conclusion, we studied various quantum interference effects in the intersubband transitions of an IR-coupled *n*-doped QW. The results showed that when two laser fields with similar Rabi frequencies couple three conduction subbands, coherent population trapping of electrons can occur. We also studied the linear responses of the system to weak probe fields under various coupling conditions. The results showed coherent effects such as laser induced transparency and dark-line effects, and revealed how coherence destruction could occur when the Rabi frequencies due to the fields became different. The natures of these coherent effects were discussed in terms of quantum interferences, and consideration was given to the role played by the dynamic evolution of the electron damping rates.

ACKNOWLEDGMENT

This research was supported by the Natural Sciences and Engineering Research Council of Canada.

[1] P. Atanasov, A. Hache, J. L. P. Hughes, H. M. van Driel, and J. E. Sipe, Phys. Rev. Lett. **76**, 1703 (1996).
[2] E. Dupont, P. B. Corkum, H. C. Liu, M. Buchanan, and Z. R. Wasilewski, Phys. Rev. Lett. **74**, 3596 (1995).
[3] S. M. Sadeghi, S. R. Leffler, and J. Meyer, Opt. Commun. **151**, 173 (1998).
[4] S. M. Sadeghi and J. Meyer (unpublished).
[5] E. Arimondo, *Progress in Optics*, edited by E. Wolf (Elsevier Science, Amsterdam, 1996), Vol. XXXV, p. 257.
[6] S. M. Sadeghi, S. R. Leffler, J. Meyer, and E. Mueller, J. Phys.: Condens. Matter **10**, 2489 (1998).
[7] J. B. Khurgin, G. Sun, L. R. Friedman, and R. A. Soref, J. Appl. Phys. **78**, 7398 (1995).
[8] F. Rossi, S. Haas, and T. Kuhn, Phys. Rev. Lett. **72**, 152 (1994); S. Hughes, A. Knorr, S. W. Koch, R. Binder, R. Indik, and J. V. Moloney, Solid State Commun. **100**, 555 (1996).
[9] J. H. Smet, C. G. Fonstad, and Q. Hu, J. Appl. Phys. **79**, 9305 (1996).
[10] J. Khurgin, J. Opt. Soc. Am. B **9**, 157 (1992).
[11] Also note that in general the exchange effects depend on the relative number of electrons in each subband (see Ref. 13), therefore, as the field intensity increases their contributions to the transition energy decrease. This shrinks the transition energy, partially compensating for the effect of the Hartree contribution, which tends to increase it.
[12] W. L. Bloss, J. Appl. Phys. **66**, 3639 (1989).
[13] A. J. Sengers, L. Tsang, and K. J. Kuhn, Phys. Rev. B **48**, 15 116 (1993).
[14] S. M. Sadeghi and J. Meyer, Phys. Rev. B **53**, 10 094 (1996).
[15] A. S. Manka, H. M. Doss, L. M. Narducci, P. Ru, and G.-L. Oppo, Phys. Rev. A **43**, 3748 (1991).
[16] H. Y. Ling, Y-Q Li, and M. Xiao, Phys. Rev. A **53**, 1014 (1996).
[17] S. M. Sadeghi, Jeff F. Young, and J. Meyer, Superlattices Microstruct. **16**, 353 (1994).
[18] S. M. Sadeghi and J. Meyer, Phys. Rev. A **58**, 2534 (1998).
[19] A. Afzali-Kushaa and G. I. Haddad, IEEE J. Quantum Electron. **QE-31**, 135 (1995).
[20] B. R. Mollow, Phys. Rev. A **5**, 2217 (1972); C. Cohen-Tannodji and S. Reynaud, J. Phys. B **10**, 345 (1977).
[21] P. L. Knight, Comments At. Mol. Phys. **15**, 193 (1984).